Temperature and doping-dependent interplay between the direct and indirect optical response in buffer-mediated epitaxial germanium

Mantu K. Hudait[1*], Michael Meeker[2], Jheng-Sin Liu[1], Michael B. Clavel[1],

Shuvodip Bhattacharya[1], and Giti A. Khodaparast[2]

[1]*Advanced Devices & Sustainable Energy Laboratory (ADSEL), Bradley Department of Electrical and Computer Engineering, Virginia Tech, Blacksburg, Virginia 24061, USA*

[2]*Department of Physics, Virginia Tech, Blacksburg, Virginia 24061, USA*

ABSTRACT.

The structural and optical properties of buffer mediated epitaxial germanium (Ge) layer were investigated and compared with bulk *n*-type and *p*-type Ge substrates. An interconnected dual-chamber molecular beam epitaxy (MBE) system was used to grow a 280 nm thin Ge epilayer on (100)GaAs substrate with an intermediate AlAs buffer layer. The lattice-matched, abrupt Ge/AlAs heterointerface was analyzed using cross-sectional transmission electron microscopic analysis, and no elemental interdiffusion was detected *via* secondary ion mass spectrometry. A strong direct gap transition, compared to the indirect gap transition, and a series of phonon-assisted transitions was observed by photoluminescence (PL) spectroscopy. In addition, the intensity of the direct gap recombination decreases with decreasing PL measurement temperatures, which was ascribed to the reduced density of Γ-valley electrons available for recombination at lower temperature. Furthermore, the intensity ratio between the direct and indirect optical transition drastically decreases with decreasing temperature in both *n*-type epitaxial and *p*-type bulk Ge. An empirical relation in both direct and indirect peak position with temperature was established. The observed strong luminescence in 280 nm thick epitaxial Ge at room temperature is vital for Ge-based photonic devices. In addition, the quality of the epitaxial Ge layer grown via MBE is on par with bulk Ge substrates.

KEYWORDS: *Germanium, Photoluminescence, Molecular beam epitaxy, Photonic devices*

*Contact author: Tel: (540) 231-6663, Fax: (540) 231-3362, E-mail: mantu.hudait@vt.edu

1. Introduction

In recent years, there has been a renewed technological interest in germanium (Ge) for light emission due to its pseudo-gap of 120 meV between the indirect L and direct Γ-valleys [1-22] in the conduction band, spurred by modifying the band structure *via* tin-alloying (Sn) [14, 16, 23-27], incorporating strain [5, 28-30], or doping. Additionally, the 2× and 4× increase in bulk electron and hole mobilities compared to Si, as well as Ge's narrow bandgap, has fostered rapid progress toward realizing ultra-low power transistors using Ge. Motivated by the possibility of integrating Ge electronic devices with Si, as along with Ge-based light emission sources for communications, several approaches have been implemented to create a direct or quasi-direct bandgap Ge, namely: (i) tensile strained Ge as-deposited on Si [22] induced *via* thermal expansion coefficient mismatch; (ii) tin alloying with Ge [14, 16, 23-27]; (iii) flexible Ge membranes [31-33]; and (iv), III-V compound semiconductor-based strain templates underneath the Ge layer [5, 34-41]. These methods have been shown to enhance the optical emission from Ge, wherein both electrically- and optically-pumped lasing from Ge [25-28, 42-44] have been demonstrated. Moreover, the recent demonstration of an electronic-photonic system-on-a-chip Si microprocessor and 1.183 μm off-chip solid-state laser source has encouraged the semiconductor industry toward the development of Ge-based light sources that could be monolithically integrated onto Si microprocessors in the near future [45]. The direct integration of the epitaxial Ge or $Ge_{1-y}Sn_y$ layer onto Si creates the defects and dislocations in the Ge layer due to ~ 4% lattice mismatch between the Ge and the Si substrate. This lattice mismatch induced defects and dislocations complicate the identification of optical transitions and the intensity of the optical emission [44, 46, 47]. In light of the above, the optical quality of any Ge material is an important benchmark. This can be achieved by growing epitaxial Ge layer on lattice matched GaAs substrate or an AlAs intermediate buffer layer. Chia *et al* [10, 11] demonstrated that an ultrathin AlAs or $Al_xGa_{1-x}As$ intermediate layer at

the GaAs/Ge heterointerface can dramatically block the cross-diffusion of Ga, As, and Ge atoms, which is attributed to the higher Al-As bonding energy. In addition, this will improve the GaAs/Ge heterointerface abruptness as well as optical quality of the GaAs epitaxy on Ge by elimination of Ge-based complexes, analyzed via photoluminescence (PL) spectroscopy. Furthermore, the interfacial $Al_xGa_{1-x}As$ layer at the Ge/GaAs heteroepitaxy demonstrated higher conduction and valence band offsets between the Ge and $Al_xGa_{1-x}As$ layers, shown below, for carrier confinement than Ge on $Si_{1-y}Ge_y$ heterostructure, where the band offset value is limited 0.20 eV [48]. Moreover, the bandgap differences between the Ge and $Al_xGa_{1-x}As$ layer can also offer a higher difference in refractive indices for carrier and optical confinement than SiGe/Si system. Therefore, the current approach of growing epitaxial Ge on GaAs with intermediate AlAs layer offers at least 3 advantages: (i) lattice matched system for minimizing defects and dislocations, (ii) larger band offsets and (iii) superior carrier and optical confinement than Ge-on-Si system. Hence, buffer mediated Ge epilayer on GaAs substrate with an intermediate AlAs layer is important for optical properties of Ge layer, and compared these properties with bulk Ge substrate are utmost important. However, evaluation of the optical properties of Ge is complicated due to the self-same 120 meV separation between the L- and Γ-valley conduction band minima, resulting in inter-valley carrier transfer, as well as the multiple phonon-assisted recombination pathways present in Ge [2, 46]. Additionally, increased PL excitation power and *n*-type dopant incorporation further confound straight-forward analysis of Ge optical properties. Thus, one metric for successful Ge epitaxy would be the demonstration of optical properties similar to that of bulk Ge, wherein any substantial differences could help to identify the differences in optical transitions between bulk (*i.e.*, vendor-supplied substrates) and epitaxial Ge materials.

In this paper, we have investigated the PL properties of epitaxially-grown, unintentionally-doped *n*-type Ge (~4×10^{18} cm^{-3}), *p*-type bulk Ge substrate (2×10^{16} cm^{-3}), and two *n*-type bulk Ge

(6×10^{16} cm^{-3}; 3×10^{17}cm^{-3}) substrates, as a function of temperature and laser excitation power during measurement. **Table I** shows the selected samples studied herein. We have observed direct and indirect recombination peaks, along with a series of phonon-assisted transitions related to

TABLE I. List of samples studied for this work.

Epitaxial Ge	Bulk *Ge*		
280 nm *n*-Ge ($4\text{x}10^{18}$ cm^{-3})	*n*-Ge ($6\text{x}10^{16}$ cm^{-3})	*n*-Ge ($3\text{x}10^{17}$ cm^{-3})	*p*-Ge ($2\text{x}10^{16}$ cm^{-3})

transverse optical (TO), longitudinal acoustic (LA) and transverse acoustics (TA) phonons. These phonon-assisted transition peaks were reduced for the epitaxially grown undoped *n*-type Ge layer, where the most likely optical transition was from the Γ-valley conduction band minimum and the valence band. We posit that the room temperature luminescence is due to the dominance of Γ-valley to valence band transitions, as opposed to L-valley to valence band transitions, regardless of whether Ge is grown on Si, AlAs, or GaAs substrates, or in its bulk (substrate) form, owing to the large absorption coefficient of Ge at the Γ-valley. The temperature and doping dependent ratios of integrated (normalized) areal intensity of direct (I_{dir}) to indirect (I_{indir}) optical transitions were also established. This ratio was found to decrease with a decrease in measurement temperature, as expected, since less carriers were available at the Γ-valley at lower temperatures. In addition, the I_{dir}/I_{indir} ratio was decreased in *p*-type bulk Ge substrates compared to epitaxial *n*-type Ge, was attributed to the low carrier density of the *p*-type Ge substrate. Lastly, we have established empirical relationships for the indirect and direct bandgap change as a function of temperature for the specimens investigated herein.

2. Experimental

The epitaxial, unintentionally-doped (*uid*) 280 nm Ge epilayers were grown on (100)GaAs substrates with an intermediate AlAs buffer layer using solid-source molecular beam epitaxy

(MBE) at a 400ºC growth temperature and a ~0.1 Å/s growth rate. Ultra-high vacuum (UHV)-interconnected Ge and III-V MBE growth chambers were used for this work. In addition, the UHV-interconnected transfer chamber prevented the surface oxidation of the AlAs buffer prior to the Ge epilayer growth. GaAs substrate oxide desorption was performed at 750ºC with a ~10^{-5} Torr arsenic (As_2) over pressure prior to growth. After the oxide desorption, undoped 250 nm GaAs and 170 nm AlAs layers were grown at 650ºC (measured by thermocouple) within the III-V MBE chamber, followed by the 280 nm Ge epilayer growth within the UHV-interconnected Ge MBE chamber. A 400 gm capacity SUMO effusion cell was used for Ge material. After growth, the samples were characterized using several analytical tools, such as cross-sectional transmission electron microscopy (TEM) and energy-dispersive x-ray spectroscopy (EDS) using a JEOL 2100 TEM system operating in scanning TEM mode for the elemental analysis. Standard sample preparation techniques were used for preparation of the cross-sectional TEM specimens, as reported earlier [34, 36]. Secondary-ion mass spectrometry (SIMS) analysis was also performed in order to determine the elemental depth profiles of Ge, Al, Ga, and As, using a Cameca IMS-7f GEO system. Temperature (77 K – 293 K) and excitation-dependent PL measurements were performed using a Ti:Sapphire laser (wavelength of 700 nm) with a repetition rate of 80 MHz, a pulse duration of ~140 fs and a spot size of ~200 µm. The pulse energy of ~ 5 nJ, determined from the maximum power, was used during measurement. The excitation light was sent through a 0.55 m focal length spectrometer, and collected by a liquid nitrogen-cooled InGaAs detector, using a standard lock-in detection scheme with a chopper frequency of ~331 Hz. In order to determine the temperature precisely, a temperature sensor was mounted next to each sample and continuous liquid nitrogen flow was maintained during measurement to avoid increase in sample temperature due to excitation of laser. Curve fitting was performed by Origin Pro® software using a convolution

of Lorentzian and Gaussian peaks. Finally, an *n*-type carrier density of ~$4x10^{18}$ cm^{-3} was measured *via* Hall-effect using a Van der Pauw geometry with evaporated metal contacts on *uid* Ge layers. Similar steps were followed for the bulk *n*-type and *p*-type Ge substrates in order to determine their carrier densities.

3. Results and Discussion

Figure 1(a) shows a representative cross-sectional schematic for the lattice matched Ge/AlAs/GaAs heterostructure grown for this work, whereas **Figs. 1(b)-(c)** show the cross-sectional TEM micrograph of the heterostructure and its elemental depth profiles, respectively. Likewise, **Fig. 1(d)** shows the dynamic SIMS analysis on a representative region of the *uid*

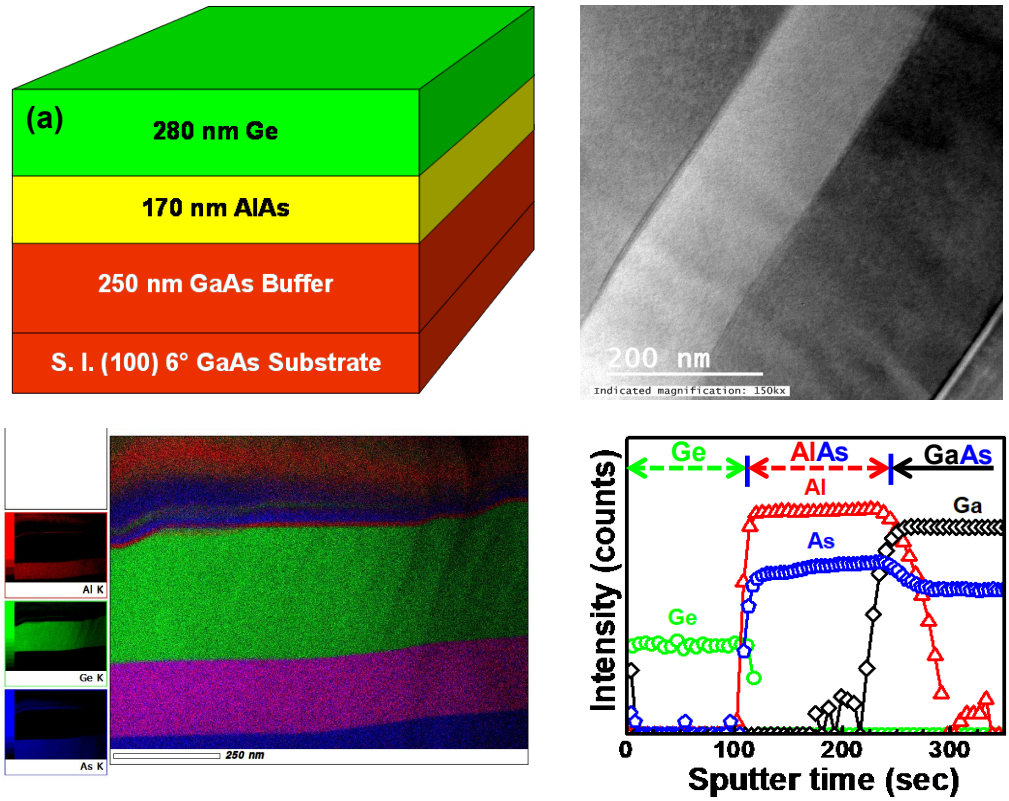

Figure 1: (a) Cross-sectional schematic of the Ge/AlAs/GaAs heterostructure, (b)-(c) cross-sectional TEM micrograph of the Ge/AlAs/GaAs heterostructure and its elemental depth profile, and (d) SIMS sputter-depth profile of the Ge/AlAs/GaAs heterostructure, where Ge, Al, Ga, and As ions measure the qualitative compositional profile as a function of sputter time (depth in the ⟨001⟩ growth direction).

Ge/AlAs/GaAs heterostructure. From **Figs. 1(b)-(c)**, one can find a sharp contrast at each heterointerface growth, in which no growth-induced defects were generated, as expected since the entire heterostructure was lattice-matched. As seen in **Fig. 1(c)**, the elemental color mappings of Ge, Al, and Ga atomic species were also clearly distinct, wherein green corresponds to the Ge content, red corresponds to the Al content, and blue corresponds to the As content. The sharp transition between regions is indicative of an abrupt transition between the Ge/AlAs and AlAs/GaAs heterointerfaces, as corroborated by the cross-sectional TEM analysis. The apparent bending at each heterointerface in **Fig. 1(c)** corresponds to a measurement artifact induced by bending of the TEM specimen during imaging. As can be seen in **Fig. 1(d)**, constant elemental Ge, Al, As, and Ga intensities (within their respective epilayers) indicate a high degree of compositional uniformity within the as-grown heterostructure. We note that the apparent Al signal detected in the GaAs epilayer and Ga signal at the surface of the Ge layer was due to a mass interference. Likewise, the apparent change in As intensity when transitioning between the AlAs and GaAs epilayers was ascribed to matrix effects on the secondary-ion mass yield during SIMS sputter depth profiling; particularly so, as no change in As_2 flux was made during growth. Additionally, no interatomic diffusion (within the sensitivity limits of dynamic SIMS analysis) was observed between group IV and III-V elemental species within the bulk of their respective epilayers. The apparent variable interdiffusion window at the AlAs/GaAs interface was ascribed to cascade mixing between elemental species during sputter depth profiling as well as the matrix effects previously discussed [49]. Moreover, recently, we have demonstrated no quantifiable atomic interdiffusion beyond an initial 6 Å interfacial width at the boron-doped Ge/AlAs heterointerface *via* atom probe tomography analysis [50]. Thus, having studied the material and structural properties of the as-grown Ge/AlAs/GaAs(001) heterostructures in question, we turn our attention towards their optical properties in comparison with bulk *n*- and *p*-type Ge substrates.

Figure 2 shows the experimental valence band (VB) and conduction band (CB) offsets between all epitaxial Ge and GaAs [49], AlAs [51], $Al_{0.5}Ga_{0.5}As$ layers, probed via x-ray photoelectron spectroscopy. Both CB and VB offsets were found to higher than GeSi/Ge system [52], needed for both carrier and optical confinement for Ge-based photonics.

The PL spectra observed in our Ge samples at room temperature and 483 mW laser power (~ 4.8 nJ pulse energy) are displayed in **Fig. 3**. From all of the samples studied in this work, two transitions were clearly visible, along with phonon replicas whose energy with respect to the L-valley conduction band minimum are indicated in **Fig. 3**. The lower energy peak was attributed to indirect recombination from the L-valley, and the higher energy peak to direct recombination from the Γ-valley. Additionally, the solid lines represent the allowed phonon-assisted transitions, whereas the dotted lines represent phonon-assisted recombination pathways not possible due to (phonon) momentum conservation restrictions. The nature of the phonon replicas is similar between the thin-film epitaxial Ge sample grown by MBE and the bulk *n*-type or *p*-type Ge substrates. One can find that the peak energy located at 0.690 eV is almost identical for all samples irrespective of sample type or doping density. Due to room temperature measurements, the PL peak is indeed a convolution of various phonon-assisted transitions, including two-phonon-assisted transitions, that mask the ability to resolve a specific transition. On the other hand, the

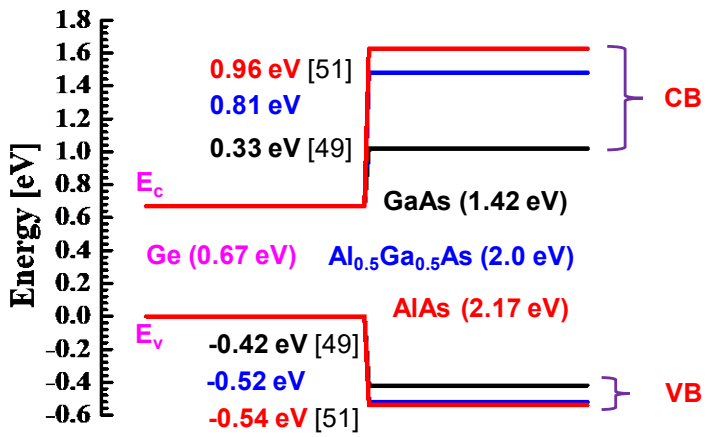

Figure 2: Conduction band (CB) and valence band (VB) offsets between all epitaxial Ge and GaAs [49], AlAs [51] and $Al_{0.5}Ga_{0.5}As$ layers. The higher band offsets were probed at the Ge/$Al_xGa_{1-x}As$ system than SiGe/Si system [52], where the CB and VB offsets total is limited to 0.20 eV.

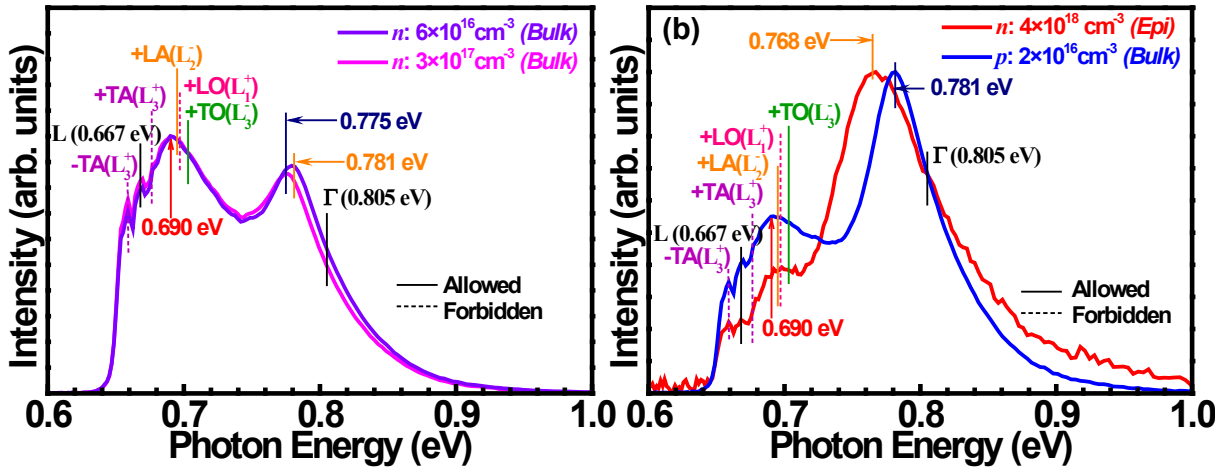

Figure 3: Room temperature PL spectra of (a) bulk *n*-type Ge substrates with two different doping densities, and (b) unintentionally doped epitaxial *n*-type Ge and bulk *p*-type Ge measured at 483 mW laser power, respectively. Direct (Γ) and indirect (L) bandgap related peak energies and associated phonon replicas have been explicitly indicated. The allowed and forbidden transitions are represented by solid and dashed line, respectively. The expected peak position related to each allowed or forbidden is shown by vertical line.

direct transition peak from the thin film Ge sample shows a shift of 13 meV with respect to the low-doped bulk *n*-type or *p*-type Ge substrates, which is attributed to doping-induced bandgap narrowing (BGN). Moreover, the indirect transition peak intensities of the *n*-type bulk Ge samples (violet and pink, **Fig. 3a**) are higher than the direct transitions. This was due to the lower electron concentration of the *n*-type bulk Ge samples, thereby limiting inter-valley scattering between the Γ- and L-valleys and reducing direct-gap recombination efficiency. On the other hand, the epitaxial thin film Ge (red) and *p*-type bulk Ge (blue) exhibited higher ratios between the direct transition from Γ-valley and the indirect transition from L-valley. This might be due to the better light extraction from the epitaxial Ge thin film, where the AlAs acts as a bottom barrier, and band offsets (conduction band and valence band, **Fig. 2)** between the Ge and the AlAs epilayers provide for increased electro-optical confinement within the Ge epilayer [38, 51]. In addition, both *p*-type bulk

Ge:Ga and the *n*-type epitaxial thin-film Ge exhibited direct emission peak intensities higher than those of the indirect peak (**Fig. 3b**).

Figure 4 shows the measured, temperature-dependent PL spectra for the (a) Ge:*uid*, heterostructure (*n*-type, with $N_D = 4\times10^{18}$ cm^{-3} as determined *via* Hall transport analysis at $T = 300$ K) and (b) *p*-type Ge:Ga substrate ($p = 2\text{x}10^{16}$ cm^{-3}). **Fig. 4(c)** shows the direct peak energy as a function of laser power excitation. One can find from **Fig. 4(a)** that two transitions were observed between 77 K and 298 K; explicitly, those associated with direct (higher energy, green) and indirect (lower energy, blue) recombination between the Γ- and L-valleys, respectively, and the Ge valence band. In addition, the intensity of the direct recombination peak in the Ge:*uid* heterostructure decreased to quasi-noise levels at temperatures approaching 77 K (Fig. 4a), a behavior that has been likewise observed in PL spectra from *p*-Ge on Si [47] and tensile-strained *n*-Ge grown directly on Si [21] This decrease in direct recombination emission stems from a lack of sufficient thermal energy to promote inter-valley scattering between the L-valley electrons and empty states in the Γ-valley, thereby reducing the density of Γ-valley electrons available for recombination, as previously discussed. The increased direct peak intensity at 298 K is due to the increase in electron concentration, which acts to fill L-valley states (prior to optical excitation), thereby reducing the energy threshold required for momentum-conserving electron scattering into available Γ-valley states. This increase in electron state filling in *n*-type Ge materials is well-understood to correspond to greatly enhanced PL intensity [9, 21].

Similarly, the temperature-dependent PL spectra recorded from the *p*-Ge:Ga substrate (**Fig. 4(b))** also exhibited a reduction in direct-gap emission intensity and an enhancement in indirect emission. The apparent increase in direct transition intensity between 178 K and 128 K (*see* Fig. 4b) was ascribed to the superposition of the increased intensity indirect peak with that of the slightly reduced intensity direct peak. For Ge:*uid* ($n = 4\times10^{18}$ cm^{-3}), the observed direct transition

occurred at 0.77 eV at T = 298 K, which is within the theoretical BGN range (27 meV) for the measured electron concentration [53, 54], shown in **Fig. 5**. A discrepancy was observed, however, between the theoretical BGN of the *p*-Ge:Ga substrate (7 meV) [54] and the experimentally determined BGN of 24 meV, corresponding to a direct transition likewise occurring at 0.77 eV. This difference could be attributed to the significant generation of optically-induced holes, as well as self-absorption effects, which would preferentially absorb higher-energy photons. In order to

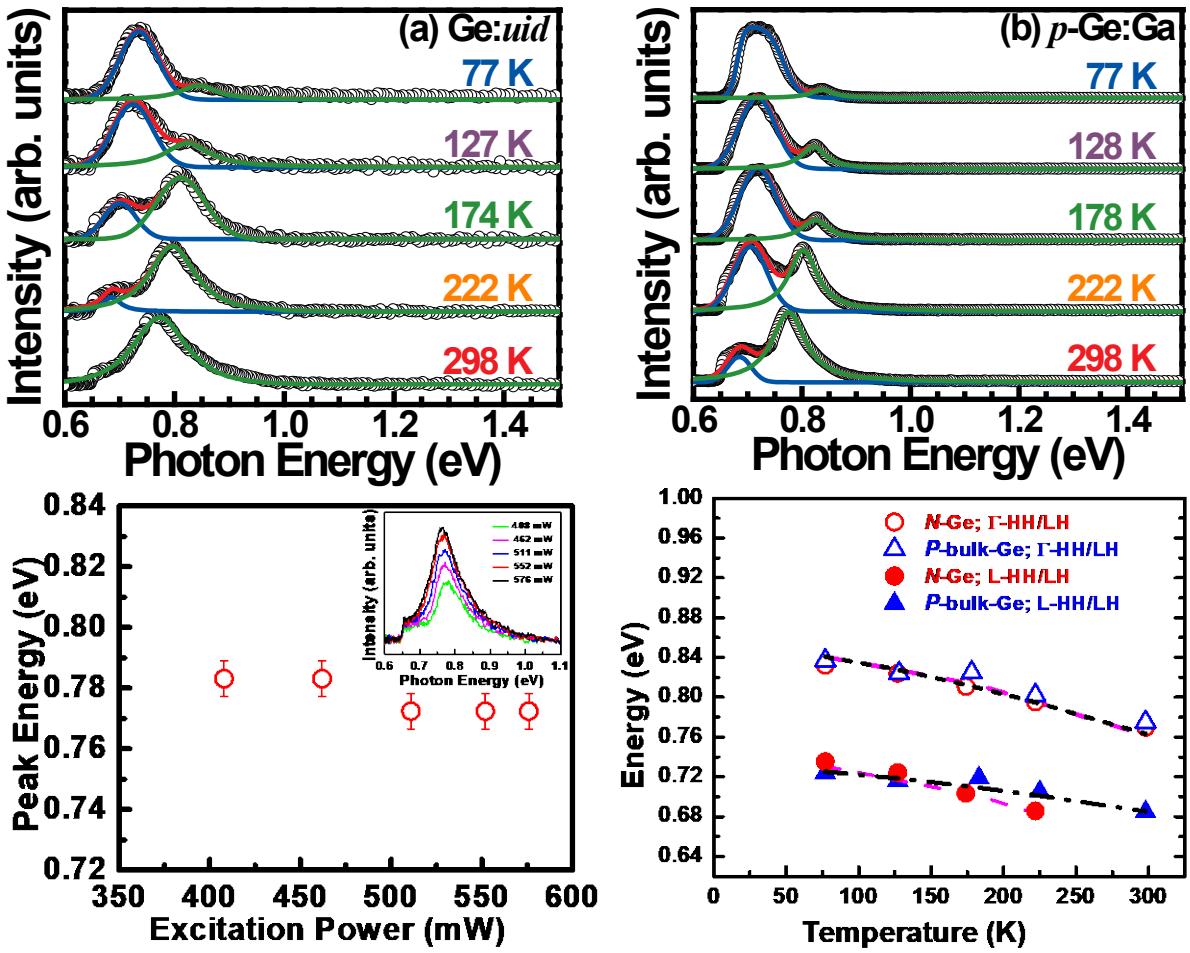

Figure 4: Temperature-dependent PL spectra from (a) *uid* *n*-type Ge, and (b) bulk *p*-type Ge:Ga measured at 573 mW laser power (~ 5.7 nJ pulse energy), respectively. (c) Room temperature peak energy of the direct-gap emission as a function of laser excitation power. (d) Direct and indirect bandgap peak energies from (a) and (b) as a function of temperature from 77 K to 298 K. The fitting related to each sample and peak energy as a function of temperature was calculated using Varshni's equation.

determine the temperature-dependence of the optical bandgaps in these two samples (*p*-type bulk Ge and epitaxial *n*-Ge), the empirical direct and indirect peak positions were fit to the Varshni equation, the results of which are tabulated in **Table II**, and graphically depicted in **Fig. 4(d)**. The direct-to-indirect intensity ratio is decreased with decreasing PL measurement temperatures for both the *n*-type Ge epilayer and *p*-type Ge substrate. However, the rate of decrease in the intensity ratios is much larger in *n*-type Ge (40×) epilayers than in the *p*-type Ge substrate (16×). This was attributed to a reduction in the electron density available in the Γ-valley at lower temperatures. These results also demonstrated an efficient radiative recombination in Ge at 298 K, as compared to 77 K, which is an essential requirement for Ge-based photonics [55]. Furthermore, the empirical relation shown in **Table II** for the direct and indirect peak positions shows an excellent fit to the data points obtained at different measurement temperatures.

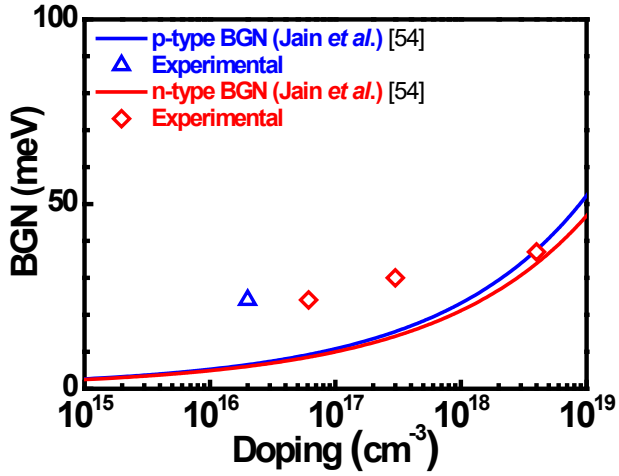

Figure 5: Model [54] and experimental bandgap narrowing (BGN) of *n*-type (red) and *p*-type bulk Ge (blue) along with epitaxial thin film *n*-type Ge (red) as a function of doping density. The experimentally determined BGN value for epitaxial thin film *n*-Ge is within the predicted value via modeling. Since the doping densities of bulk-Ge samples are low, there is an error between the experimental and the predicted value.

TABLE II. Temperature and doping dependent ratio of integrated (normalized) areal intensity of direct (I_{dir}) to indirect (I_{indir}) optical transitions. The symbol "--" indicates that no measurable indirect optical transition could be observed.

T (K)	*n*-Ge (~4x10^{18} cm^{-3})			Bulk *p*-Ge (~2x10^{16} cm^{-3})		
	I_{dir}	I_{indir}	I_{dir}/I_{indir}	I_{dir}	I_{indir}	I_{dir}/I_{indir}
298	0.169	--	--	0.118	0.019	6.06
222	0.152	0.009	16.65	0.083	0.072	1.16
174, 178	0.132	0.033	3.94	0.028	0.087	0.32
127, 128	0.055	0.086	0.64	0.026	0.084	0.31
77	0.033	0.079	0.41	0.006	0.093	0.07
	$E_g^{\Gamma}(T) = 0.85 - \frac{5.9\times10^{-4}T^2}{(296+T)}$ eV $E_g^{L}(T) = 0.747 - \frac{6.1\times10^{-4}T^2}{(296+T)}$ eV			$E_g^{\Gamma}(T) = 0.85 - \frac{5.8\times10^{-4}T^2}{(296+T)}$ eV $E_g^{L}(T) = 0.73 - \frac{3\times10^{-4}T^2}{(296+T)}$ eV		

4. Conclusions

We have grown and analyzed the structural and optical properties of epitaxial Ge on GaAs substrates with an intermediate AlAs buffer layer. Cross-sectional TEM analysis, along with *in-situ* elemental profiling, demonstrated a lattice-matched heterointerface, as expected, since the entire structure is quasi-lattice matched. Within the detection limit of SIMS, minimal or no interdiffusion of Ge, Al, As, and Ga elements were detected, corroborated by the lower Ge growth temperature and growth rate, as discussed above. In addition, we have analyzed the luminescence features of epitaxial, thin-film Ge and compared the results with both *n*-type and *p*-type bulk Ge substrates. While analyzing luminescence results, we observed a strong direct gap transition, as compared to the indirect gap transition, as well as a series of phonon-assisted transitions. Comparing the shape of the optical spectrum at room temperature from 280 nm epitaxial *n*-type Ge and bulk *p*-type Ge substrates, we can exclude the self-absorption effect in Ge. Moreover, the observed strong luminescence in Ge at room temperature is vital for Ge-based photonic devices going forward. The intensity of the direct gap was also observed to decrease with decreasing PL

measurement temperatures, which was ascribed to the reduced density of Γ-valley electrons available for recombination at lower temperatures. Furthermore, the intensity ratio between the direct and indirect optical transitions drastically decreased with decreasing temperature in both *n*-type epitaxial and *p*-type bulk Ge. Finally, we have established an empirical relation in both direct and indirect peak positions with temperature, wherein the change in bandgap trends for both indirect- and direct-gap emission peaks were almost identical. In addition, the quality of the epitaxial Ge layer grown via MBE is on par with bulk Ge substrates. These results thereby suggest the suitability of leveraging epitaxial Ge grown on large bandgap III-V buffers towards the integration of Ge-based electronics and photonics on silicon.

Acknowledgements

M. C. and M. K. H. acknowledges partial support from the NSF under grant number ECCS-1507950 and ECCS-2042079, a US-Ireland joint R&D program. The authors acknowledge the NCFL - Institute for Critical Technology and Applied Science and Virginia Tech Nanofabrication facilities for assistance with the materials characterization. G. K. and M. M. acknowledge the support of the AFOSR through grant FA9550-14-1-0376 and FA9550-17-1-0341.

Data availability. The data that support the findings of this study are available from the corresponding author upon reasonable request.

References

[1] S. –H. Tang, E. Y. Chang, M. K. Hudait, J. –S. Maa, C. –W. Liu, G. –L. Luo, H. –D. Trinh, and Y. –H. Su, High quality Ge thin film grown by ultrahigh vacuum chemical vapor deposition on GaAs substrate, Appl. Phys. Lett. 98 (2011) 161905. https://doi.org/10.1063/1.3580605

[2] R. R. Lieten, K. Bustillo, T. Smets, E. Simoen, J. W. Ager III, E. E. Haller, and J. –P. Locquet, Photoluminescence of bulk germanium, Phys. Rev. B 86 (2012) 035204. https://doi.org/10.1103/PhysRevB.86.035204

[3] T. Arguirov, M. Kittler, and N. V. Abrosimov, Room temperature luminescence from Germanium, J. Physics: Conf. Ser. 281 (2011) 012021. https://doi.org/10.1088/1742-6596/281/1/012021

[4] T. –H. Cheng, C. –Y. Ko, C. –Y. Chen, K. –L. Peng, G. –L. Luo, C. W. Liu, and H. –H. Tseng, Competitiveness between direct and indirect radiative transitions of Ge, Appl. Phys. Lett. 96 (2010) 091105. https://doi.org/10.1063/1.3352048

[5] Y. Bai, K. E. Lee, C. Cheng, M. L. Lee, and E. A. Fitzgerald, Growth of highly tensile-strained Ge on relaxed InxGa1-xAs by metal-organic chemical vapor deposition, J. App. Phys. 104 (2008) 084518. https://doi.org/10.1063/1.3005886

[6] T. –H. Cheng, K. –L. Peng, C. –Y. Ko, C. –Y. Chen, H. –S. Lan, Y. –R. Wu, C. W. Liu, and H. –H. Tseng, Strain-enhanced photoluminescence from Ge direct transition, Appl. Phys. Lett. 96 (2010) 211108. https://doi.org/10.1063/1.3429085

[7] M. El Kurdi, H. Bertin, E. Martincic, M. de Kersauson, G. Fishman, S. Sauvage, A. Bosseboeuf, and P. Boucaud, Control of direct band gap emission of bulk germanium by mechanical tensile strain, Appl. Phys. Lett. 96 (2010) 041909. https://doi.org/10.1063/1.3297883

[8] J. Wagner, and L. Viña, Radiative recombination in heavily doped p-type germanium, Phys. Rev. B 30 (1984) 7030. https://doi.org/10.1103/PhysRevB.30.7030

[9] M. El Kurdi, T. Kociniewski, T. –P. Ngo, J. Boulmer, D. Débarre, P. Boucaud, J. F. Damlencourt, O. Kermarrec, and D. Bensahel, Enhanced photoluminescence of heavily n-doped germanium, Appl. Phys. Lett. 94, (2009) 191107. https://doi.org/10.1063/1.3138155

[10] C. K. Chia, G. K. Dalapati, Y. Chai, S. L. Lu, W. He, J. R. Dong, D. H. L. Seng, H. K. Hui, A. S. W. Wong, A. J. Y. Lau, Y. B. Cheng, D. Z. Chi, Z. Zhu, Y. C. Yeo, Z. Xu, and S. F. Yoon, Role of AlxGa1-xAs buffer layer in heterogeneous integration of GaAs/Ge, J. Appl. Phys. 109 (2011) 066106. https://aip.scitation.org/doi/10.1063/1.3561489

[11] C. K. Chia, J. R. Dong, D. Z. Chi, A. Sridhara, A. S. W. Wong, M. Suryana, G. K. Dalapati, S. J. Chua, and S. J. Lee, Effects of AlAs interfacial layer on material and optical properties of GaAs⁄Ge(100) epitaxy, Appl. Phys. Lett. 92 (2008) 141905. https://doi.org/10.1063/1.2908042

[12] Y. Cai, Z. Han, X. Wang, R. E. Camacho-Aguilera, L. C. Kimerling, J. Michel, and J. Liu, Analysis of Threshold Current Behavior for Bulk and Quantum-Well Germanium Laser Structures, IEEE J. Sel. Top. Quantum Electron. 19 (2013) 1901009. 10.1109/JSTQE.2013.2247573

[13] Z. Wang, A. Abbasi, U. Dave, A. De Groote, S. Kumari, B. Kunert, C. Merckling, M. Pantouvaki, Y. Shi, B. Tian, K. Van Gasse, J. Verbist, R. Wang, W. Xie, J. Zhang, Y. Zhu, J. Bauwelinck, X. Yin, Z. Hens, J. Van Campenhout, B. Kuyken, R. Baets, G. Morthier, D. Van Thourhout, and G. Roelkens, Novel Light Source Integration Approaches for Silicon Photonics, Laser Photonics Rev. 11 (2017) 1700063. https://doi.org/10.1002/lpor.201700063

[14] A. Elbaz, D. Buca, N. von den Driesch, K. Pantzas, G. Patriarche, N. Zerounian, E. Herth, X. Checoury, S. Sauvage, I. Sagnes, A. Foti, R. Ossikovski, J. –M. Hartmann, F. Boeuf, Z. Ikonic, P. Boucaud, D. Grützmacher, and M. El Kurdi, M, Ultra-low-threshold continuous-wave and pulsed lasing in tensile-strained GeSn alloys, Nat. Photonics 14 (2020) 375. https://doi.org/10.1038/s41566-020-0601-5

[15] R. A. Soref, D. Buca, and S. –Q. Yu, Group IV Photonics: Driving Integrated Optoelectronics, Opt. Photon. News 27 (2016) 32. https://doi.org/10.1364/OPN.27.1.000032

[16] D. Stange, S. Wirths, R. Geiger, C. Schulte-Braucks, B. Marzban, N. von den Driesch, G. Mussler, T. Zabel, T. Stoica, J. –M. Hartmann, S. Mantl, Z. Ikonic, D. Grützmacher, H. Sigg, J. Witzens, and D. Buca, D, Optically Pumped GeSn Microdisk Lasers on Si, ACS Photonics 3 (2016) 1279. https://doi.org/10.1021/acsphotonics.6b00258

[17] S. Al-Kabi, S. D. Amir Ghetmiri, J. Margetis, T. Pham, Y. Zhou, W. Dou, B. Collier, R. Quinde, W. Du, A. Mosleh, J. Liu, G. Sun, R. A. Soref, J. Tolle, B. Li, M. Mortazavi, H. A. Naseem, and S. –Q. Yu, An optically pumped 2.5 μm GeSn laser on Si operating at 110 K, Appl. Phy. Lett. 109 (2016) 171105. https://doi.org/10.1063/1.4966141

[18] V. Singh, V.; P. T. Lin, N. Patel, H. Lin, L. Li, Y. Zou, F. Deng, C. Ni, J. Hu, J. Giammarco, A. Paola Soliani, B. Zdyrko, I. Luzinov, S. Novak, J. Novak, P. Wachtel, S. Danto, J. D. Musgraves, K. Richardson, L. C. Kimerling, and A. M. Agarwal, Mid-infrared materials and devices on a Si platform for optical sensing, Sci. Technol. Adv. Mater. 15 (2014) 2. https://doi.org/10.1088/1468-6996/15/1/014603

[19] S. Bao, D. Kim, C. Onwukaeme, S. Gupta, K. Saraswat, K. H. Lee, Y. Kim, D. Min,Y. Jung, H. Qiu, H. Wang, E. A. Fitzgerald, C. S. Tan, and D. Nam, Low-threshold optically pumped lasing in highly strained germanium nanowires, Nat Commun. 8 (2017) 1845. https://doi.org/10.1038/s41467-017-02026-w

[20] N. von den Driesch, D. Stange, S. Wirths, G. Mussler, B. Holländer, Z. Ikonic, J. M. Hartmann, T. Stoica, S. Mantl, D. Grützmacher, and D. Buca, Direct Bandgap Group IV Epitaxy on Si for Laser Applications, Chem. Mater. 27 (2015) 4693. https://doi.org/10.1021/acs.chemmater.5b01327

[21] X. Sun, J. Liu, L. C. Kimerling, and J. Michel, Direct gap photoluminescence of n-type tensile-strained Ge-on-Si, Appl. Phys. Lett. 95 (2009) 011911. https://doi.org/10.1063/1.3170870

[22] A. Ghosh, M. Clavel, P. Nguyen, M. Meeker, G. Khodaparast, R. Bodnar, and M. K. Hudait, Growth, structural, and electrical properties of germanium-on-silicon heterostructure by molecular beam epitaxy, AIP Advances 7 (2017) 095214. https://doi.org/10.1063/1.4993446

[23] Y. Zhou, W. Dou, W. Du, S. Ojo, H. Tran, S. A. Ghetmiri, J. Liu, G. Sun, R. Soref, J. Margetis, J. Tolle, B. Li, Z. Chen, M. Mortazavi, and S. –Q. Yu, Optically Pumped GeSn Lasers Operating at 270 K with Broad Waveguide Structures on Si, ACS Photonics 6 (2019) 1434. https://doi.org/10.1021/acsphotonics.9b00030

[24] E. M. T. Fadaly, A. Dijkstra, J. R. Suckert, D. Ziss, M. A. J. van Tilburg, C. Mao, Y. Ren, V. T. van Lange; K. Korzun, S. Kölling, M. A. Verheijen, D. Busse, C. Rödl, J. Furthmüller, F. Bechstedt, J. Stangl, J. J. Finley, S. Botti, J. E. M. Haverkort, and E. P. A. M. Bakkers, Direct-bandgap emission from hexagonal Ge and SiGe alloys, Nature 580 (2020) 205. 10.1038/s41586-020-2150-y

[25] J. Liu, X. Sun, R. Camacho-Aguilera, L. C. Kimerling, and J. Michel, Ge-on-Si laser operating at room temperature, Opt. Lett. 35 (2010) 679. https://doi.org/10.1364/OL.35.000679

[26] B. R. Dutt, D. S. Sukhdeo, D. Nam, B. M. Vulovic, Z. Yuan, and K. C. Saraswat, Roadmap to an Efficient Germanium-on-Silicon Laser: Strain vs. n-Type Doping, IEEE J. Photonics 4 (2012) 2002. https://doi.org/10.1109/JPHOT.2012.2221692

[27] S. Wirths, R. Geiger, N. von den Driesch, G. Mussler, T. Stoica, S. Mantl, Z. Ikonic, M. Luysberg, S. Chiussi, J. M. Hartmann, H. Sigg, J. Faist, D. Buca, and D. Grutzmacher, Lasing in direct-bandgap GeSn alloy grown on Si, Nat. Photonics 9 (2015) 88. https://doi.org/10.1038/nphoton.2014.321

[28] W. W. Chow, Model for direct-transition gain in a Ge-on-Si laser, Appl. Phys. Lett. 100 (2012) 191113. https://doi.org/10.1063/1.4714540

[29] M. El Kurdi, G. Fishman, S. Sauvage, and P. Boucaud, Band structure and optical gain of tensile-strained germanium based on a 30 band k·p formalism, J. Appl. Phys. 107 (2010) 013710. https://doi.org/10.1063/1.3279307

[30] J. F. Liu, X. Sun, D. Pan, X. X. Wang, L. C. Kimerling, T. L. Koch, and J. Michel, Tensile-strained, n-type Ge as a gain medium for monolithic laser integration on Si, Opt. Express 15 (2007) 11272. https://doi.org/10.1364/OE.15.011272

[31] J. R. Sanchez-Perez, C. Boztug, F. Chen, F. F. Sudradjat, D. M. Paskiewicz, R. B. Jacobson, M. G. Lagally, and R. Paiella, Direct-bandgap light-emitting germanium in tensilely strained nanomembranes, Proc. Natl. Acad. Sci. U. S. A. 108 (2011) 18893. https://doi.org/10.1073/pnas.1107968108

[32] K. Guilloy, N. Pauc, A. Gassenq, Y. –M. Niquet, J. –M. Escalante, I. Duchemin, S. Tardif, G. O. Dias, D. Rouchon, J. Widiez, J. –M. Hartmann, R. Geiger, T. Zabel, H. Sigg, J. Faist, A. Chelnokov, V. Reboud, and V. Calvo, Germanium under High Tensile Stress: Nonlinear Dependence of Direct Band Gap vs Strain, ACS Photonics 3 (2016) 1907. https://doi.org/10.1021/acsphotonics.6b00429

[33] M. J. Suess, R. Geiger, R. A. Minamisawa, G. Schiefler, J. Frigerio, D. Chrastina, G. Isella, R. Spolenak, J. Faist, and H. Sigg, Analysis of enhanced light emission from highly strained germanium microbridges, Nat. Photonics 7 (2013) 466. https://doi.org/10.1038/nphoton.2013.67

[34] M. Clavel, D. Saladukha, P. Goley, T. J. Ochalski, F. Murphy-Armando, R. J. Bodnar, and M. K. Hudait, Heterogeneously-Grown Tunable Tensile Strained Germanium on Silicon for Photonic Devices, ACS Appl. Mater. Inter. 7 (2015) 26470. https://doi.org/10.1021/acsami.5b07385

[35] M. Clavel, P. S. Goley, N. Jain, Y. Zhu, and M. K. Hudait, Strain-Engineered Biaxial Tensile Epitaxial Germanium for High-Performance Ge/InGaAs Tunnel Field-Effect Transistors, IEEE J. Elec. Dev. Soc. 3 (2015) 184. https://doi.org/10.1109/JEDS.2015.2394743

[36] Y. Zhu, D. Maurya, S. Priya, and M. K. Hudait, Tensile-Strained Nanoscale Ge/$In_{0.16}Ga_{0.84}As$ Heterostructure for Tunnel Field-Effect Transistor, ACS Appl. Mater. Inter. 6 (2014) 4947. https://doi.org/10.1021/am405988f

[37] D. Saladukha, M. B. Clavel, F. Murphy-Armando, G. Greene-Diniz, M. Gruening, M. K. Hudait, T. J. Ochalski, Direct and indirect band gaps in Ge under biaxial tensile strain investigated by photoluminescence and photoreflectance studies, Phys. Rev. B 97 (2018) 195304. https://doi.org/10.1103/PhysRevB.97.195304

[38] M. K. Hudait, M. Clavel, P. Goley, Y. Xie, and J. J. Heremans, Magnetotransport Properties of Epitaxial Ge/AlAs Heterostructures Integrated on GaAs and Silicon, ACS Appl. Mater. Inter. 7 (2015) 22315. https://doi.org/10.1021/acsami.5b05814

[39] J. R. Jain, A. Hryciw, T. M. Baer, D. A. B. Miller, M. L. Brongersma, and R. T. Howe, A micromachining-based technology for enhancing germanium light emission via tensile strain, Nat. Photonic 6 (2012) 398. https://doi.org/10.1038/nphoton.2012.111

[40] M. Qi, C. A. Stephenson, V. Protasenko, W. A. O'Brien, A. Mintairov, H. Xing, and M. A. Wistey, Ge quantum dots encapsulated by AlAs grown by molecular beam epitaxy on GaAs without extended defects, Appl. Phys. Lett. 104 (2014) 073113. https://doi.org/10.1063/1.4866278

[41] D. Jung, J. Faucher, S. Mukherjee, A. Akey, D. J. Ironside, M. Cabral, X. Sang, J. Lebeau, S. R. Bank, T. Buonassisi, O. Moutanabbir, and M L. Lee, Highly tensile-strained Ge/InAlAs nanocomposites, Nat. Commun. 8 (2017) 14204. https://doi.org/10.1038/ncomms14204.

[42] M. E. Groenert, C. W. Leitz, A. J. Pitera, V. Yang, H. Lee, R. J. Ram, and E. A. Fitzgerald, Monolithic integration of room-temperature cw GaAs/AlGaAs lasers on Si substrates via relaxed graded GeSi buffer layers, J. Appl. Phys. 93 (2003) 362. https://doi.org/10.1063/1.1525865

[43] R. E. Camacho-Aguilera, Y. Cai, N. Patel, J. T. Bessette, M. Romagnoli, L. C. Kimerling, and J. Michel, An electrically pumped germanium laser, Opt. Express 20 (2012) 11316. https://doi.org/10.1364/OE.20.011316

[44] J. Liu, X. Sun, L. C. Kimerling, and J. Michel, Direct-gap optical gain of Ge on Si at room temperature, Opt. Lett. 34 (2009) 1738. https://doi.org/10.1364/OL.34.001738

[45] C. Sun, M. T. Wade, Y. Lee, J. S. Orcutt, L. Alloatti, M. S. Georgas, A. S. Waterman, J. M. Shainline, R. R. Avizienis, S. Lin, B. R. Moss, R. Kumar, F. Pavanello, A. H. Atabaki, H. M. Cook, A. J. Ou, J. C. Leu, Y. –H. Chen, K. Asanović, R. J. Ram, M. A. Popović, and V. M. Stojanović, Single-chip microprocessor that communicates directly using light, Nature 528 (2015) 534. https://doi.org/10.1038/nature16454

[46] G. Grzybowski, R. Roucka, J. Mathews, L. Jiang, R. T. Beeler, J. Kouvetakis, and J. Menendez, Direct versus indirect optical recombination in Ge films grown on Si substrates. Phys. Rev. B 84 (2011) 205307. https://doi.org/10.1103/PhysRevB.84.205307.

[47] M. –Y. Ryu, T. R. Harris, Y. K. Yeo, R. T. Beeler, and J. Kouvetakis, Temperature-dependent photoluminescence of Ge/Si and $Ge_{1-y}Sn_y$/Si, indicating possible indirect-to-direct bandgap transition at lower Sn content, Appl. Phys. Lett. 102 (2013), 171908. https://doi.org/10.1063/1.4803927

[48] S. Adachi, in Properties of Semiconductor Alloys: Group-IV, III–V, and II–VI Semiconductors, edited by P. Capper, S. Kasap, and A. Willoughby (Wiley, New York, 2009), pp. 275–283. https://doi.org/10.1002/978047074369.ch9

[49] M. K. Hudait, Y. Zhu, N. Jain, and J. L. Hunter, Jr., Structural, morphological, and band alignment properties of GaAs/Ge/GaAs heterostructures on (100), (110), and (111)A GaAs substrates, J. Vac. Sci. Technol. B31 (2013) 011206. https://doi.org/10.1116/1.4770070

[50] M. B. Clavel, G. Green-Diniz, M. Gruning, K. T. Henry, M. Kuhn, R. J. Bodnar, and M. K. Hudait, Engineering the Interfacial Electronic Structure of Epitaxial Ge/AlAs(001) Heterointerfaces via Substitutional Boron Incorporation: The Roles of Doping and Interface Stoichiometry, ACS Appl. Electron. Mater. 1 (2019) 2646. https://doi.org/10.1021/acsaelm.9b00615

[51] M. K. Hudait, M. Clavel, P. Goley, N. Jain, and Y. Zhu, Heterogeneous Integration of Epitaxial Ge on Si using AlAs/GaAs Buffer Architecture: Suitability for Low-power Fin Field-Effect Transistors, Sci. Rep. 4 (2014) 6964. https://doi.org/10.1038/srep06964

[52] R. Pillarisetty, B. Chu-Kung, S. Corcoran, G. Dewey, J. Kavalieros, H. Kennel, R. Kotlyar, V. Le, D. Lionberger, M. Metz, N. Mukherjee, J. Nah, W. Rachmady, M. Radosavljevic, U. Shah, S. Taft, H. Then, N. Zelick, and R. Chau, High mobility strained germanium quantum well field effect transistor as the p-channel device option for low power (Vcc=0.5V) III-V CMOS architecture, *IEDM Technical Digest* 2010, pp. 150-153. https://doi.org/10.1109/IEDM.2010.5703312

[53] C. Haas, Infrared Absorption in Heavily Doped n-Type Germanium, Phys. Rev. 125 (1962) 1965. https://doi.org/10.1103/PhysRev.125.1965

[54] S. Jain, and J. D. Roulston, A simple expression for band gap narrowing (BGN) in heavily doped Si, Ge, GaAs and Ge_xSi_{1-x} strained layers, Solid-State Electron. 34 (1991) 453. https://doi.org/10.1016/0038-1101(91)90149-S

[55] M. K. Hudait, F. Murphy-Armando, D. Saladukha, M. B. Clavel, P. S. Goley, D. Maurya, S. Bhattacharya, T. J. Ochalski, Theoretical and Experimental Investigation of Tensile-Strained Germanium Quantum-Well Laser Structure, ACS Appl. Electron. Mater. 3 (2021) 4535-4547. https://doi.org/10.1021/acsaelm.1c00660